Ciliary ARL13B is essential for body weight regulation in adult mice

Tiffany T. Terry[a], Eduardo D. Gigante[a, b, c], Coralie M. Alexandre[d], Kathryn M. Brewer[e], Xinyu Yue[d], Nicolas F. Berbari[e], Christian Vaisse[d], Tamara Caspary[a, f]

[a] Department of Human Genetics, Emory University School of Medicine, Atlanta, GA, 30322

[b] Graduate Program in Neuroscience, Laney Graduate School, Emory University, Atlanta, GA, 30322

[c] Present address: Department of Molecular and Cellular Biology, Kennesaw State University, Kennesaw, GA, 30144

[d] Diabetes Center and Department of Medicine, University of California, San Francisco, San Francisco, CA, 94143

[e] Department of Biology, Indiana University- Indianapolis, Indianapolis, IN, 46202

[f] Address correspondence to: Tamara Caspary (tcaspar@emory.edu), 404-727-9862

ORCID and email for authors:

Tiffany T. Terry 0000-0002-2729-6281, tiffany.terry@emory.edu

Eduardo D. Gigante 0000-0002-1486-5377, egigante@kennesaw.edu

Coralie M. Alexander 0009-0004-2978-2648 Coralie.Alexandre@ucsf.edu

Kathryn M. Brewer 0009-0006-3498-4492 katmbrew@iu.edu

Xinyu Yue 0000-0002-6187-5906 Xinyu.Yue@ucsf.edu

Nicolas F. Berbari 0000-0003-2863-1069 nberbari@iu.edu

Christian Vaisse 0000-0003-4274-7033 Christian.Vaisse@ucsf.edu

Tamara Caspary 0000-0002-6579-7589, tcaspar@emory.edu

Abstract

Cilia are near ubiquitous cellular appendages critical for cell-to-cell communication and involved in diverse developmental and homeostatic processes. ARL13B is a regulatory GTPase enriched in cilia. We engineered an *Arl13b* mouse allele, *Arl13b*^{V358A}, which retains ARL13B biochemical activities but renders ARL13B undetectable in cilia. Surprisingly, these mice are hyperphagic and become obese and insulin resistant. In addition to its GTPase function, ARL13B acts as a guanine nucleotide exchange factor (GEF) for ARL3. To test whether ARL13B's GEF activity is required to regulate body weight, we analyzed the body weight of mice expressing an ARL13B variant lacking ARL3 GEF activity (*Arl13b*^{R79Q}). We found no difference in body weight, indicating ARL13B is unlikely to regulate weight via its ARL3 GEF activity. Ciliary ARL13B could control energy homeostasis through a role in development or in adult mice. We induced wildtype ARL13B expression, which localizes to cilia, in 4-week-old *Arl13b*$^{V358A/V358A}$ mice and found the obesity phenotype and associated metabolic impairments were rescued, consistent with ARL13B regulating homeostatic signaling within cilia in adult mice. These results show that ciliary ARL13B functions to control body weight. Our ability to genetically control the subcellular localization of ARL13B by removing and introducing it into cilia enables us to define the cilia-specific role of ARL13B and provides key information for understanding how cilia act as a signaling hub critical for energy homeostasis.

Author Summary

Primary cilia are essential for energy homeostasis, and their disruption leads to syndromic obesity. However, the mechanisms by which ciliary components regulate energy balance remain unclear. Here, we identify a key role for the ciliary GTPase ARL13B in energy homeostasis. Using a mouse model expressing the ARL13B^{V358A} variant, which is excluded from cilia but retains biochemical activity, we show that ciliary ARL13B regulates body weight, as *Arl13b*$^{V358A/V358A}$ mice become obese and hyperphagic. Remarkably, restoring ciliary ARL13B in

these mice rescues obesity, demonstrating its crucial role in acute ciliary signaling for energy balance. This study directly links ciliary ARL13B with energy balance in adult animals.

Introduction

Arl13b, an ADP-ribosylation factor (ARF) protein family member, encodes a regulatory GTPase highly enriched on the ciliary membrane[1, 2]. Like other regulatory GTPases, ARL13B has multiple functions, likely mediated by distinct effectors. For example, it has a conserved role as a guanine nucleotide exchange factor (GEF) for ARL3[3, 4]. In cilia, ARL13B regulates retrograde intraflagellar transport as well as the phospholipid composition of the ciliary membrane[5-7]. In mice, loss of ARL13B is embryonic lethal, disrupting ciliogenesis and Hedgehog (Hh) signaling[8, 9]. Patient mutations in *ARL13B* cause the ciliopathy Joubert Syndrome (JS)[10, 11]. JS patients present with developmental delay, intellectual disability, and physical anomalies, and all known causative *ARL13B* mutations disrupt ARL13B's GEF activity for ARL3[4].

We engineered an ARL13B mouse variant (ARL13B^{V358A}) that maintains the known biochemical functions of ARL13B but is undetectable in cilia[12]. Surprisingly, these mice display normal Hh signaling but retain the ciliogenesis defects seen in the null allele[12]. These data argue that cellular ARL13B regulates Hh, and ciliary ARL13B controls ciliogenesis. Thus, homozygous *Arl13b*$^{V358A/V358A}$ mice (hereafter called *Arl13b*$^{A/A}$) reveal ciliary ARL13B function, after embryonic development and in adult animals.

Outside of JS, several other ciliopathies cause metabolic abnormalities and obesity. Alstrom (ALMS) syndrome and Bardet-Biedl syndrome (BBS) are among the ciliopathies in which obesity is a major clinical feature[13-15]. For example, loss of function mutations in *ALMS1* lead to defects in cilia assembly and function, impacting ciliation and ciliary signaling in cells that

regulate appetite and energy balance[16-18]. BBS mutations disrupt cilia protein import and export, impacting ciliary signaling and trafficking of proteins involved in regulating food intake and energy metabolism[19-22]. In adult mice, genetic ablation of cilia causes obesity due to hyperphagia and leads to elevated levels of leptin, glucose, and insulin[23, 24]. Loss of cilia on specific neuronal cell types during development also results in hyperphagia-associated obesity[23, 25, 26]. Together, these findings show that primary cilia are required for regulating energy homeostasis. Yet, these approaches have been unable to distinguish the cilia-specific roles of proteins compared to their functions in other parts of the cell. Understanding the role of cilia-mediated signaling in obesity will likely uncover mechanisms driving common forms of obesity.

Here, we report that *Arl13b*$^{A/A}$ mice become hyperphagic and obese, indicating that the cilia-specific function of ARL13B is critical for energy homeostasis regulation. ARL13B's GEF activity for ARL3 is unlikely to be required to regulate body weight as mice expressing a variant (*Arl13b*^{R79Q}) that lacks *in vitro* ARL13B GEF activity for ARL3 are not overweight. Rescuing ciliary ARL13B in 4-week-old *Arl13b*$^{A/A}$ mice prevents obesity, suggesting ARL13B controls body weight through a homeostatic role in ciliary signaling. These findings demonstrate that ciliary ARL13B is essential for body weight regulation in adult mice and provides a molecular entry point for understanding the complex roles ciliary signaling plays in adult energy homeostasis.

Results

ARL13B^{V358A} *protein is undetectable in primary cilia in adult mouse tissues*

The engineered ARL13B^{V358A} variant disrupts ARL13B from localizing to primary cilia in mouse embryonic fibroblasts, neural tube, and kidneys[12, 27, 28] (**Figure 1 A** and **B**). To assess

whether ARL13B^{V358A} protein is in cilia in cell types previously implicated in ciliopathy-associated metabolic phenotypes, we performed immunofluorescence staining for ARL13B and the neuronal cilia marker adenylate cyclase 3 (ADCY3) in the hypothalamus and endocrine pancreas[29, 30]. In the hypothalamus, we detected ADCY3 staining in the arcuate (ARC), the paraventricular (PVN), and the ventromedial (VMH) hypothalamic nuclei, indicating the presence of neuronal cilia. In control mice, ARL13B co-localizes with ADCY3 in the ARC, the PVN, and VMH, indicating it is normally present in cilia (**Figure 1 C**, **E**, **G**). However, we could not detect the ARL13B signal in neuronal cilia in these brain regions of *Arl13b*$^{A/A}$ mice, indicating the engineered variant does not enrich in these cilia (**Figure 1 D**, **F**, **H**). In the ARC, appetite-stimulating agouti-related peptide (AgRP)-expressing neurons and the appetite-suppressing pro-opiomelanocortin (POMC)-expressing neurons are key regulators of food intake[31]. To assess whether loss of ciliary ARL13B disrupted the number or patterning of AgRP and POMC neurons in the ARC, we performed RNAscope in situ hybridization. We found normal frequency and patterning for both AgRP and POMC neurons in the ARC of *Arl13b*$^{A/A}$ mice, indicating ciliary ARL13B does not play a role in the hypothalamic patterning of these cell types (**Supplemental Figure 1 A-D**).

To determine whether ARL13B^{V358A} protein is detectable on pancreatic islet cells, we performed immunofluorescence staining for ARL13B, acetylated α-tubulin, glucagon (α-cells), and insulin (β-cells). We observed ARL13B co-localizes with acetylated α-tubulin on α- and β-cells in the cilia of control mice but not on pancreatic islet cells in *Arl13b*$^{A/A}$ mice (**Supplemental Figure 2 A-D**). These findings demonstrate that ciliary ARL13B is present in both the hypothalamic feeding centers and pancreatic islets of adult mice, but in mice expressing the ARL13B^{V358A} variant, ARL13B is undetectable in cilia.

Arl13b$^{A/A}$ mice are obese, hyperphagic, and insulin-resistant

Whereas the *Arl13b*$^{hnn/hnn}$ null mice are embryonic lethal, homozygous *Arl13b*$^{A/A}$ survive into adulthood and display an increased body weight compared to wildtype (*Arl13b*$^{+/+}$) control littermates[8]. To investigate their body weight profile, we generated longitudinal data from weaning (week 3) to adult (week 10). We found no significant differences in body weight curves among the control genotypes: *Arl13b*$^{+/+}$, *Arl13b*$^{+/A}$, and *Arl13b*$^{+/hnn}$ in male and female mice, indicating the mutations are recessive and display no evidence of a gain-of-function (e.g. dominant negative) effect. The *Arl13b*$^{A/A}$ mice became significantly heavier than all control genotypes at week 5 for males and week 7 for females (**Figure 2 A** and **B**). By week 10, both male and female *Arl13b*$^{A/A}$ mice were, on average, 30% heavier than controls.

Arl13b$^{A/A}$ mice are obese, as the increase in weight was exclusively attributed to an increase in fat mass. Body composition analysis showed comparable lean mass between *Arl13b*$^{A/A}$ and control animals (**Figure 2 C** and **H**). The difference in body weight between the two genotypes was characterized by a 123% increase in fat mass in male *Arl13b*$^{A/A}$ mice and a 158% increase in fat mass in female *Arl13b*$^{A/A}$ mice (**Figure 2 D** and **I**). Consistent with the increase in fat mass, we also observed increased leptin levels in *Arl13b*$^{A/A}$ mice (**Figure 2 E** and **J)**.

To evaluate whether the *Arl13b*$^{A/A}$ weight phenotype is sensitive to *Arl13b* gene dosage, we bred the *Arl13b*^{A} allele with the null *Arl13b*^{hnn} allele. We weighed male and female *Arl13b*$^{A/hnn}$ heterozygous mice from weeks 3 to 10. We found that *Arl13b*$^{A/hnn}$ mice displayed a similar body weight phenotype to *Arl13b*$^{A/A}$ mice, indicating that less overall ARL13B protein had no impact on this phenotype (**Figure 2 A** and **B**).

To examine whether the obesity phenotype is the result of changes in feeding, we measured food intake from weeks 4 to 5, just prior to when we first observed an increase in *Arl13b*$^{A/A}$ body weight. We found that male and female *Arl13b*$^{A/A}$ mice consumed, on average, ~20% more food per day compared to littermate controls (**Figure 2 F** and **K**). To investigate whether changes in activity and/or metabolism contribute to the increased body weight in

Arl13b$^{A/A}$ mice, we measured energy expenditure using a Comprehensive Lab Animal Monitoring System (CLAMS). Male *Arl13b*$^{A/A}$ mice displayed a modest 13% increase in daily energy expenditure (**Figure 2G)**. Females showed no changes in energy expenditure compared to control animals (**Figure 2L**). These data demonstrate that the increase in body weight we observe in male and female *Arl13b*$^{A/A}$ mice is due to hyperphagia.

We further determined whether excluding ARL13B from cilia influenced glycemic regulation. *Arl13b*$^{A/A}$ mice were hyperinsulinemic (**Figure 3 A** and **B**) and normoglycemic (**Figure 3 C-F**) at baseline, suggesting conserved insulin production by beta-cells. During glucose tolerance tests, both male and female *Arl13b*$^{A/A}$ mice exhibited elevated blood glucose levels, but these were only significant in females (**Figure 3 C** and **D**). Insulin did not lower blood glucose levels in male and female *Arl13b*$^{A/A}$ mice compared to controls, revealing an insulin-resistance phenotype consistent with the changes we observed in body composition (**Figure 3 E** and **F**). Together, these data indicate that *Arl13b*$^{A/A}$ mice are hyperinsulinemic, glucose intolerant, and insulin resistant, congruent with their obese phenotype.

ARL13B's GEF activity for ARL3 does not appear to regulate energy homeostasis

One possible mechanism of ARL13B action within cilia is via its GEF activity for ARL3, which would imply that activated ARL3 is involved in energy homeostasis regulation[3, 4, 32, 33]. This predicts that the obesity we observed upon restricting ARL13B from cilia in *Arl13b*$^{A/A}$ mice would be recapitulated by disrupting ARL13B's function via its GEF activity for ARL3. To test this directly, we examined mice in which we modified the endogenous *Arl13b* locus to express only the ARL13B variant *Arl13b*^{R79Q}, which lacks *in vitro* GEF activity for ARL3 [4, 34] (**Figure 1A)**. We found that *Arl13b*$^{R79Q/R79Q}$ mice displayed normal body weight (**Figure 4 A** and **B**). While we cannot exclude the possibility of a compensatory GEF for ARL3, these findings suggest that the obesity phenotype in *Arl13b*$^{A/A}$ mice is likely independent of ARL13B's GEF activity.

Introducing ciliary ARL13B in 4-week-old Arl13b$^{A/A}$ mice prevents obesity

Ciliary ARL13B could control energy homeostasis through a role in development or in adult mice. To address this, we induced expression of wildtype ARL13B, which localizes to cilia, after development and tracked the body weight profile of the animals. We used a Cre-inducible *Arl13b-Fucci2a* (*AF2a*) allele that expresses wildtype ARL13B fused to a Cerulean fluorophore[35]. We crossed *Arl13b$^{A/A}$;AF2a* mice to *CAGG-CreER^{T2}* transgenic mice in which Cre is ubiquitously activated following tamoxifen induction (**Figure 5A**). We confirmed that ARL13B-Cerulean is present in cilia only after Cre recombination (**Figure 5 B** and **C**). ARL13B-Cerulean co-localizes with the neuronal marker ADCY3 in the ARC, the PVN, and the VMH in tamoxifen-treated *Arl13b$^{A/A}$;AF2a;CAGG-CreER^{T2}* mice but not in tamoxifen-treated *Arl13b$^{A/A}$* mice lacking Cre (**Supplemental Figure 3 A-F**).

We longitudinally tracked the impact of including ARL13B-Cerulean expression at 4-weeks in *Arl13b$^{A/A}$;AF2a;CAGG-CreER^{T2}* mice (referred to hereafter as *Arl13b$^{A/A}$;AF2a$^{CAGG\text{-}4wk}$*) compared to controls *Arl13b$^{+/A}$;AF2a;CAGG-CreER^{T2}* and *Arl13b$^{A/A}$* mice. From week 8 until week 12, both male and female *Arl13b$^{A/A}$; AF2a$^{CAGG\text{-}4wk}$* mice weighed significantly less than *Arl13b$^{A/A}$* mice (**Figure 5 D** and **E**). These data demonstrate that ciliary ARL13B plays a role after development is complete and suggest that ARL13B regulates acute signaling in cilia to control body weight.

To examine the homeostatic response of *Arl13b$^{A/A}$;AF2a$^{CAGG\text{-}4wk}$* mice to glucose and insulin, we performed glucose and insulin tolerance tests in 13 to 15-week-old mice. In response to glucose, male and female *Arl13b$^{A/A}$;AF2a$^{CAGG\text{-}4wk}$* mice cleared glucose from their bloodstream, similar to control mice, while *Arl13b$^{A/A}$* mice displayed elevated blood glucose levels (**Figure 5 F** and **G**). In response to insulin, the blood glucose levels in male *Arl13b$^{A/A}$;AF2a$^{CAGG\text{-}4wk}$* mice trended with the levels in control animals (**Figure 5H**). In contrast, insulin lowered blood glucose levels in female *Arl13b$^{A/A}$;AF2a$^{CAGG\text{-}4wk}$* mice (**Figure 5I**). These data demonstrate that introducing wildtype ARL13B in cilia of *Arl13b$^{A/A}$* mice normalizes

glycemic regulation, showing that ARL13B must be in cilia for normal glucose and insulin metabolism.

Discussion

Our study identifies a cilia-specific role of ARL13B as a critical regulator of energy homeostasis. Mice expressing the cilia-excluded variant, ARL13B^{V358A}, become hyperphagic, obese, and insulin resistant soon after weaning. We also demonstrate that ARL13B's role in energy homeostasis is independent of its GEF activity for ARL3. Finally, we show that the obesity phenotype can be rescued by introducing ciliary ARL13B after weaning, demonstrating it does not play a developmental role and suggesting ciliary ARL13B likely regulates energy homeostasis via an acute signaling role in the adult. Together, these data reveal that ciliary ARL13B is essential for food intake and body weight regulation in adult mice.

While ARL13B^{V358A} is an engineered mutation, we were surprised to observe obesity in *Arl13b*$^{A/A}$ mice as distinct patient mutations in *ARL13B* lead to JS[10, 11]. JS is clinically defined by its neurodevelopmental features, including the diagnostic molar tooth structure on an MRI, as well as developmental delay, breathing abnormalities, and abnormal eye movements; it is not typically associated with obesity. Consistent with this, we did not observe a weight phenotype in mice expressing the JS-causing variant, ARL13B^{R79Q}. It is notable that one JS patient with obesity carried an ARL13B^{Y86C} mutation. However, it is not clear that the mutation caused the obesity. The ARL13B^{Y86C} mutation, like ARL13B^{R79Q}, lacks GEF activity for ARL3. That said, there are clear links between cilia and obesity[36, 37]. These include ciliopathies like BBS and ALMS or mutations in the G-protein-coupled receptor melanocortin receptor 4 (MC4R), which localizes to cilia[38, 39]. Thus, the cilia-specific role of ARL13B in controlling energy homeostasis may involve interactions with other ciliopathy proteins or signaling machinery.

We conclude that ARL13B's GEF activity for ARL3 is unlikely to be required for energy homeostasis. We base this on analysis of the ARL13B^{R79Q} mutation. The full-length, recombinant mouse protein purified from HEK cells lacks any evidence of *in vitro* GEF activity for ARL3[4]. It is worth noting that when a bacterially expressed, truncated protein that included the homologous mutation (R77Q) in the Chlamydomonas ortholog of ARL13B, GEF activity decreased compared to wild type, but residual activity was present[40]. Reasons for this apparent discrepancy (absent vs reduced GEF activity) could result from a number of differences, including the use of mouse vs Chlamydomonas proteins (which share only 29.5% identity) or the source of protein expression (mammalian vs bacterial). In any case, the analysis of the mammalian protein directly reflects the consequences of this point mutation in mouse. It is possible that the R79Q mutation disrupts additional ARL13B function. R79 plays an important role in the conformational stability of ARL13B's switch II region, commonly used to bind effectors. The mutation to glutamine (R79Q) in our mouse could alter binding not only to the effector ARL3, for which it has GEF activity, but also to other unrecognized effectors. We also cannot formally exclude the possibility of a compensatory GEF for ARL3 in vivo.

Given ARL13B's well-documented roles in development and the neural developmental features of JS, we sought to determine whether ciliary ARL13B regulates developmental processes. We first assessed whether there were developmental patterning phenotypes of the hypothalamus that led to hyperphagia-associated obesity. Our analysis showed no overt changes in cell population numbers within the ARC (POMC and AgRP). Additionally, we induced expression of wild-type ARL13B-Cerulean at 4 weeks of age in *Arl13b*$^{A/A}$ mice and observed a rescue of the obesity phenotype. Collectively, these data indicate that ciliary ARL13B is not regulating developmental processes to control energy homeostasis and are consistent with ciliary ARL13B controlling acute signaling in adult animals. While the ARL13B-Cerulean induction was ubiquitous, we note that the hypothalamic circuits that control feeding

are established by four weeks of age, which is just prior to the significant weight gain we observe in *Arl13b*$^{A/A}$ mice[41].

Our data clearly argue that obesity in *Arl13b*$^{A/A}$ animals is driven by hyperphagia and increased fat mass. The hyperphagic phenotype just before significant weight gain in *Arl13b*$^{A/A}$ mice strongly suggests the involvement of hypothalamic neurons. We observed that ARL13B is normally in cilia on neurons in multiple hypothalamic feeding centers and on pancreatic islet cells, but absent from cilia on these cell types in *Arl13b*$^{A/A}$ mutants. We eliminated two alternative possibilities for the weight phenotype. First, we previously reported that *Arl13b*$^{A/A}$ mice develop progressive, mild kidney cysts[28]. However, the size and rate of kidney cyst progression in these animals do not account for the changes in body weight and composition we observe. Second, we showed that the weight phenotype does not depend on gene dosage, as including the *Arl13b*^{hnn} null allele did not impact weight. Similarly, we found that ARL13B overexpression using the inducible *Arl13b-Cerulean* allele did not impact weight[42].

One possible mechanism through which ciliary ARL13B regulates energy homeostasis involves the established interaction between ARL13B and INPP5E in the ciliary membrane[6, 7, 32]. Patients lacking the C-terminal CaaX domain of INPP5E lose INPP5E ciliary localization and exhibit MORM syndrome, which includes obesity[43]. INPP5E is not detected in the cilia of *Arl13b*$^{A/A}$ cells, consistent with data showing that the ciliary retention of INPP5E depends on ARL13B. Thus, the loss of ciliary INPP5E in the absence of ciliary ARL13B could impact the trafficking or signaling of proteins implicated in feeding behavior, such as MC4R. This would suggest the obesity-causing ARL13B^{V358A} mutation functions via INPP5E, whereas JS-causing mutations in ARL13B act via ARL3. While a tantalizing model, it is challenging to reconcile with *INPP5E* mutations causing JS or the finding that INPP5E requires activated ARL3 (ARL3-GTP) to enter cilia.

Our *Arl13b*$^{A/A}$ model isolates the ciliary role of the ARL13B protein. This model enables us to directly interrogate, at a subcellular resolution, how ARL13B controls cilia-mediated signaling pathways involved in maintaining energy homeostasis. A slight sex difference was observed in the glucose homeostasis phenotype. This phenotype could be studied further once the anatomical and cellular basis for ciliary Arl13b-dependent obesity has been identified. Our data indicate that ARL13B typically localizes to cilia in tissues that regulate energy homeostasis. The absence of ARL13B from cilia in these tissues leads to obesity, suggesting a critical role for ciliary ARL13B in body weight control. Future studies will identify the cell type or combination of cells that require ciliary ARL13B function and the mechanism of ciliary ARL13B action to regulate energy homeostasis.

Materials and Methods

Ethics Statement

All mice were cared for in accordance with NIH guidelines, and animal experimental procedures were approved by the Institutional Animal Care and Use Committees (IACUC) at Emory University (20170058), the University of California, San Francisco (AN201856), and Indiana University-Indianapolis (SC358R).

Mouse lines. Mice were housed in a barrier facility and maintained on a 12:12 light cycle (from 7 a.m. to 7 p.m.) at an ambient temperature of 23°C ± 2°C and relative humidity of 50%–70%. Mice were fed with rodent diet 5058 (Lab Diet) and group housed (up to 5 mice per cage). Lines used were *Arl13b*^{V358A} (C57BL/6J-*Arl13b*^{em1Tc}) [MGI: 6256969], *Arl13b*^{R79Q} (C57BL/6J-*Arl13b*^{em2Tc}) [MGI: 6279301], and *Arl13b-Fucci2a* [MGI:6193732][(35)]. Mice were genotyped for the V358A mutation using primers MB11: 5'-CCTATATTCTTCTAGAAAA-CAGTAAGAAGAAAACCAAGAAACTAAGACTCCTTTTCATTCATCGGGC-3' and MB12: 5'-

GACAGTAAAGGATTCTTCCTCACAACCTGAC-3' to detect the mutant allele, and primers MB21: 5'-CTTAAGATGACTTTGAGTTTGGAAGAAATACAAGATAGC-3' and MB22: 5'-GCGTGGGACTCTTTGGAGTAGACTAGTCAATACAGACGGGTTCTA-3' to detect the wildtype allele. Band sizes were 395bp for wildtype and 273bp for mutant. Mice were genotyped for the R79Q mutation using primers 223_2F: 5'-TCACTTGCAACAGAGCATCC-3' and 223_2R: 5'-ACAGCTCTGCCCGTGTTTAC-3' followed by Sanger sequencing the 304bp PCR product. Mice were genotyped for the *Arl13b-Fucci2a* allele using primers F: 5'- AAAACCTCCCACACCTCCC -3' and R: 5'- CGACCATCACAAGTGTCACC -3'.

Mouse metabolism studies. Mice were single-housed for 7 days, and food was weighed daily. The average daily food weight between groups was taken. Energy expenditure was measured by the Comprehensive Lab Animal Monitoring System (CLAMS, Columbus Instruments, Columbus, Ohio). Mice were tested over 96 continuous hours, and the data from the last 48 hours were analyzed. Kilocalories per hour were calculated using the Lusk equation: Energy Expenditure = (3.815 + 1.232 × respiratory exchange ratio [RER]) × oxygen consumption rate (VO_2) and analyzed with CalR software[44] (ANCOVA with body weight used as a covariate). Lean mass and fat mass were measured using the EchoMRI™ system[45].

Glucose tolerance test. Adult mice were fasted for 16 hours and injected with 1 g/kg body weight glucose intraperitoneally (Sigma G7021). Blood glucose was measured at 0, 10, 20, 30, 60, 90, and 120 minutes via tail sampling with the AlphaTrak3 blood glucose meter (Zoetis). A blood sample for fasting glucose levels was taken at time point 0, before glucose was injected.

Insulin tolerance test. Adult mice were fasted for 3 hours before intraperitoneal injection with 0.75 U/kg body weight regular human insulin (Humulin R, Lilly USA, and Novolin R, Novo Nordisk). Blood glucose levels were measured at 0, 15, 30, 45, and 60 minutes. A blood sample for fasting insulin levels was taken at time point 0, before insulin was administered.

Blood serum analysis. Blood was allowed to coagulate at room temperature for 30 minutes, then centrifuged at 1200 x g for 10 min at room temperature. Serum was collected and stored at -80°C. Insulin and leptin levels were measured with Crystal Chem's ultra-sensitive mouse ELISA kits according to the manufacturer's protocol (leptin: catalog # 90080 and insulin catalog # 90030).

Tamoxifen administration. Tamoxifen (Sigma T5648) stock solution was prepared at a concentration of 20mg/ml in 100% EtOH and stored at -20°C. Each dose of tamoxifen was freshly prepared in corn oil on the day of injection and dissolved using a speed vacuum centrifuge (Eppendorf Vacufuge plus). To induce gene expression, 10ul/g tamoxifen in 200ul corn oil was administered by oral gavage to 4-week-old mice using a 1ml syringe and a 22G 1.5-inch straight needle (Braintree Scientific Inc).

Tissue harvesting and preparation. Mice were euthanized with isoflurane inhalation followed by perfusion with ice-cold PBS and ice-cold 4% paraformaldehyde (PFA). Brain and pancreas tissues were harvested and post-fixed with 4% PFA overnight at 4°C. Tissues were then cryoprotected in 30% sucrose in 0.1 M phosphate buffer at 4°C until tissues sank in solution. Samples were then frozen in optimal cutting temperature compound (Tissue-Tek OCT, Sakura Finetek).

Immunohistochemistry. 12µm or 20µm cryosections were rehydrated, blocked and permeabilized in antibody wash (5% heat-inactivated goat serum, 0.1% Triton X-100 in Tris-buffered Saline) for 30-40 minutes. Tissues were incubated with primary antibodies overnight at 4°C, washed three times with 0.1% Triton X-100 in Tris-Buffered Saline (TBST), and incubated with secondary antibodies for 1 hour at room temperature. Tissues were washed three times with TBST and incubated with Hoechst 33342 for 5 minutes. Slides were coverslipped with ProLong Gold (ThermoFisher) mounting media. Slides cured overnight at room temperature in the dark and were stored long-term at -20°C. Slides were imaged on a BioTek Lionheart FX

microscope. Primary antibodies used were: mouse anti-ARL13B (1:1000, NeuroMab, N295B/66); rabbit anti-acetylated α-tubulin (1:1000,Cell Signaling, 5335); mouse anti-acetylated α-tubulin (1:2500, Sigma, T7451); chicken anti-ACIII (1:1000, Encor, CPCA-ACIII); rat anti-insulin (1:1000, R&D systems, MAB1417); rabbit anti-glucagon (1:2000, Abcam, ab92517), chicken anti-GFP (1:8000, Abcam, ab13970) recognizes cerulean. Secondary antibodies used were goat anti-mouse AlexaFluor 488, goat anti-chicken AlexaFluor 647, goat anti-chicken AlexaFluor 488, goat anti-rat AlexaFluor 568 and donkey anti-rabbit AlexaFluor 555 (all at 1:500, ThermoFisher).

RNAScope. Brains from adult mice were harvested, fixed, and prepared for RNAscope in situ hybridization[46, 47]. Briefly, 15µm cryosections were mounted on slides and then post-fixed with 4% PFA for 16hr at 4□C. Detection of transcripts was performed using the RNAscope 2.5 HD Duplex Assay (Advanced Cell Diagnostics (ACD), Newark, CA). Tissue pretreatment was performed according to technical note 320534 Rev A. Probe hybridization, counterstaining, and mounting of slides were performed according to user manual no. 322500-USM Rev A. Slides were assayed using probes to AgRP (Cat No. 400711) and POMC (Cat No. 314081) transcripts (ACD). Sections were counterstained with hematoxylin, dehydrated, and mounted using VectaMount (Vectorlabs, Burlingame, CA). Slides with positive control probe (PPIB-C1/POLR2A-C2; Cat No. 321651) and negative control probe (DapB; Cat No. 320751) were run with each experiment. (n ≥ 3 animals per group).

Funding

This work was supported by the National Institutes of Health: diversity supplement to R35GM122549 and F32DK137409 (TTT); T32NS096050, diversity supplement to R01NS090029 and F31NS106755 (EDG); Larry L. Hillblom Foundation fellowship (CMA);

University Fellowship and F31DK142351 (KMB); American Heart Association pre-doctoral fellowship (XY); R01DK114008 (NFB); R01DK124769, R01DK106404 and R01DK060540 (CV); and R01NS090029, R35GM122549 and R35GM148416 (TC).

Reference List

1. Larkins CE, Gonzalez Aviles GD, East MP, Kahn RA, Caspary T. Arl13b regulates ciliogenesis and the dynamic localization of Shh signaling proteins. Molecular Biology of the Cell. 2011;22(23):4694-703.
2. Sun Z, Amsterdam A, Pazour GJ, Cole DG, Miller MS, Hopkins N. A genetic screen in zebrafish identifies cilia genes as a principal cause of cystic kidney. Development. 2004;131(16):4085-93.
3. Gotthardt K, Lokaj M, Koerner C, Falk N, Gießl A, Wittinghofer A. A G-protein activation cascade from Arl13B to Arl3 and implications for ciliary targeting of lipidated proteins. eLife. 2015;4:1-16.
4. Ivanova AA, Caspary T, Seyfried NT, Duong DM, West AB, Liu Z, et al. Biochemical characterization of purified mammalian ARL13B protein indicates that it is an atypical GTPase and ARL3 guanine nucleotide exchange factor (GEF). Journal of Biological Chemistry. 2017;292(26):11091-108.
5. Nozaki S, Katoh Y, Terada M, Michisaka S, Funabashi T, Takahashi S, et al. Regulation of ciliary retrograde protein trafficking by the Joubert syndrome proteins ARL13B and INPP5E. Journal of Cell Science. 2017;130(3):563-76.
6. Humbert MC, Weihbrecht K, Searby CC, Li Y, Pope RM, Sheffield VC, et al. ARL13B, PDE6D, and CEP164 form a functional network for INPP5E ciliary targeting. Proceedings of the National Academy of Sciences of the United States of America. 2012;109(48):19691-6.
7. Qiu H, Fujisawa S, Nozaki S, Katoh Y, Nakayama K. Interaction of INPP5E with ARL13B is essential for its ciliary membrane retention but dispensable for its ciliary entry. Biology Open. 2021;10(1).
8. Caspary T, Larkins CE, Anderson KV. The Graded Response to Sonic Hedgehog Depends on Cilia Architecture. Developmental Cell. 2007;12(5):767-78.
9. Su CY, Bay SN, Mariani LE, Hillman MJ, Caspary T. Temporal deletion of Arl13b reveals that a mispatterned neural tube corrects cell fate over time. Development (Cambridge). 2012;139(21):4062-71.
10. Cantagrel V, Silhavy JL, Bielas SL, Swistun D, Marsh SE, Bertrand JY, et al. Mutations in the Cilia Gene ARL13B Lead to the Classical Form of Joubert Syndrome. American Journal of Human Genetics. 2008;83(2):170-9.

11. Thomas S, Cantagrel V, Mariani L, Serre V, Lee JE, Elkhartoufi N, et al. Identification of a novel ARL13B variant in a Joubert syndrome-affected patient with retinal impairment and obesity. European Journal of Human Genetics. 2015;23(5):621-7.
12. Gigante ED, Taylor MR, Ivanova AA, Kahn RA, Caspary T. ARL13B regulates Sonic Hedgehog signaling from outside primary cilia. bioRxiv. 2019:1-23.
13. Collin GB, Marshall JD, Ikeda A, So WV, Russell-Eggitt I, Maffei P, et al. Mutations in ALMS1 cause obesity, type 2 diabetes and neurosensory degeneration in Alström syndrome. Nature Genetics. 2002;31(1):74-8.
14. Forsythe E, Beales PL. Bardet-Biedl syndrome. European Journal of Human Genetics. 2013;21(1):8-13.
15. Hearn T, Spalluto C, Phillips VJ, Renforth GL, Copin N, Hanley NA, et al. Subcellular Localization of ALMS1 Supports Involvement of Centrosome and Basal Body Dysfunction in the Pathogenesis of Obesity, Insulin Resistance, and Type 2 Diabetes. Electrophoresis. 2005;54(May):1581-7.
16. Collin GB, Cyr E, Bronson R, Marshall JD, Gifford EJ, Hicks W, et al. Alms1-disrupted mice recapitulate human Alström syndrome. Human Molecular Genetics. 2005;14(16):2323-33.
17. Arsov T, Silva DG, O'Bryan MK, Sainsbury A, Lee NJ, Kennedy C, et al. Fat aussie - A new Alström syndrome mouse showing a critical role for ALMS1 in obesity, diabetes, and spermatogenesis. Molecular Endocrinology. 2006;20(7):1610-22.
18. Heydet D, Chen LX, Larter CZ, Inglis C, Silverman MA, Farrell GC, et al. A truncating mutation of Alms1 reduces the number of hypothalamic neuronal cilia in obese mice. Developmental Neurobiology. 2013;73(1):1-13.
19. Berbari NF, Lewis JS, Bishop GA, Askwith CC, Mykytyn K. Bardet-Biedl syndrome proteins are required for the localization of G protein-coupled receptors to primary cilia. 2008.
20. Domire JS, Green JA, Lee KG, Johnson AD, Askwith CC, Mykytyn K. Dopamine receptor 1 localizes to neuronal cilia in a dynamic process that requires the Bardet-Biedl syndrome proteins. Cellular and Molecular Life Sciences. 2011;68(17):2951-60.
21. Shinde SR, Nager AR, Nachury MV. Ubiquitin chains earmark GPCRs for BBSome-mediated removal from cilia. Journal of Cell Biology. 2020;219(12).
22. Ye F, Nager AR, Nachury MV. BBSome trains remove activated GPCRs from cilia by enabling passage through the transition zone. Journal of Cell Biology. 2018;217(5):1847-68.
23. Davenport JR, Watts AJ, Roper VC, Croyle MJ, van Groen T, Wyss JM, et al. Disruption of Intraflagellar Transport in Adult Mice Leads to Obesity and Slow-Onset Cystic Kidney Disease. Current Biology. 2007;17(18):1586-94.
24. Berbari NF, Pasek RC, Malarkey EB, Yazdi SMZ, McNair AD, Lewis WR, et al. Leptin resistance is a secondary consequence of the obesity in ciliopathy mutant mice.

Proceedings of the National Academy of Sciences of the United States of America. 2013;110(19):7796-801.

25. Wang Y, Bernard A, Comblain F, Yue X, Paillart C, Zhang S, et al. Melanocortin 4 receptor signals at the neuronal primary cilium to control food intake and body weight. Journal of Clinical Investigation. 2021;131(9).

26. Wang L, De Solis AJ, Goffer Y, Birkenbach KE, Engle SE, Tanis R, et al. Ciliary gene RPGRIP1L is required for hypothalamic arcuate neuron development. JCI Insight. 2019;4(3).

27. Mariani LE, Bijlsma MF, Ivanova AI, Suciu SK, Kahn RA, Caspary T. Arl13b regulates Shh signaling from both inside and outside the cilium. Molecular Biology of the Cell. 2016;27(23):3780-90.

28. Van Sciver RE, Long AB, Katz HG, Gigante ED, Caspary T. Ciliary ARL13B inhibits developmental kidney cystogenesis in mouse. Developmental Biology. 2023;500:1-9.

29. Brewer KM, Brewer KK, Richardson NC, Berbari NF. Neuronal cilia in energy homeostasis. Frontiers in Cell and Developmental Biology: Frontiers Media S.A.; 2022.

30. Bishop GA, Berbari NF, Lewis J, Mykytyn K. Type III adenylyl cyclase localizes to primary cilia throughout the adult mouse brain. Journal of Comparative Neurology. 2007;505(5):562-71.

31. De Solis AJ, Del Río-Martín A, Radermacher J, Chen W, Steuernagel L, Bauder CA, et al. Reciprocal activity of AgRP and POMC neurons governs coordinated control of feeding and metabolism. Nature Metabolism. 2024;6(3):473-93.

32. Fujisawa S, Qiu H, Nozaki S, Chiba S, Katoh Y, Nakayama K. ARL3 and ARL13B GTPases participate in distinct steps of INPP5E targeting to the ciliary membrane. Biology Open. 2021;10(9).

33. Zhang Q, Li Y, Zhang Y, Torres VE, Harris PC, Ling K, et al. GTP-binding of ARL-3 is activated by ARL-13 as a GEF and stabilized by UNC-119. Scientific Reports. 2016;6.

34. Suciu SK, Long AB, Caspary T. Smoothened and ARL13B are critical in mouse for superior cerebellar peduncle targeting. Genetics. 2021;218(4).

35. Ford MJ, Yeyati PL, Mali GR, Keighren MA, Waddell SH, Mjoseng HK, et al. A Cell/Cilia Cycle Biosensor for Single-Cell Kinetics Reveals Persistence of Cilia after G1/S Transition Is a General Property in Cells and Mice. Developmental Cell. 2018;47(4):509-23.e5.

36. Vaisse C, Reiter JF, Berbari NF. Cilia and obesity. Cold Spring Harbor Perspectives in Biology. 2017;9(7).

37. Engle SE, Bansal R, Antonellis PJ, Berbari NF. Cilia signaling and obesity. Seminars in Cell and Developmental Biology: Elsevier Ltd; 2021. p. 43-50.

38. Siljee JE, Wang Y, Bernard AA, Ersoy BA, Zhang S, Marley A, et al. Subcellular localization of MC4R with ADCY3 at neuronal primary cilia underlies a common pathway for genetic predisposition to obesity. Nature Genetics. 2018;50(2):180-5.
39. Vaisse C, Clement K, Durand E, Hercberg S, Guy-Grand B, Froguel P. Melanocortin-4 receptor mutations are a frequent and heterogeneous cause of morbid obesity. The Journal of Clinical Investigation. 2000;106(2):253-62.
40. Miertzschke M, Koerner C, Spoerner M, Wittinghofer A. Structural insights into the small G-protein Arl13B and implications for Joubert syndrome. Biochem J. 2014;457(2):301-11.
41. Bouret SG. Developmental programming of hypothalamic melanocortin circuits. Experimental and Molecular Medicine. 2022;54:403-13.
42. Long AB, Wilson IM, Terry TT, Van Sciver RE, Caspary T. ARL13B-Cerulean rescues Arl13b-null mouse from embryonic lethality and reveals a role for ARL13B in spermatogenesis. 2025.
43. Jacoby M, Cox JJ, Gayral S, Hampshire DJ, Ayub M, Blockmans M, et al. INPP5E mutations cause primary cilium signaling defects, ciliary instability and ciliopathies in human and mouse. Nature Genetics. 2009;41(9):1027-31.
44. Mina AI, LeClair RA, LeClair KB, Cohen DE, Lantier L, Banks AS. CalR: A Web-Based Analysis Tool for Indirect Calorimetry Experiments. Cell Metabolism. 2018;28(4):656-66.e1.
45. Jones AS, Johnson MS, Nagy TR. Validation of quantitative magnetic resonance for the determination of body composition of mice. International Journal of Body Composition Research. 2009;7(2):67-72.
46. Antonellis PJ, Engle SE, Brewer KM, Berbari NF. The hedgehog signaling pathway is expressed in the adult mouse hypothalamus and modulated by fasting. eNeuro. 2021;8(5).
47. Engle SE, Antonellis PJ, Whitehouse LS, Bansal R, Emond MR, Jontes JD, et al. A CreER mouse to study melanin concentrating hormone signaling in the developing brain. Genesis. 2018;56(8):1-7.

Figure Legends

Figure 1: *ARL13B*^{V358A} protein is undetectable in primary cilia in adult mouse tissues.

(**A**) Schematic of ARL13B protein domains and relevant amino acid sequence in wildtype and mutant in the cilia localization sequence (CLS). (**B**) Schematic of ARL13B (green) localization in

a wildtype (*Arl13b*$^{+/+}$), (grey) null (*Arl13b*$^{hnn/hnn}$), and cilia-excluded (*Arl13b*$^{A/A}$) models. (**C-H**) Immunofluorescence of ADCY3 (red) and ARL13B (green) in hypothalamic feeding centers PVN (**C-D**), VMH (**E-F**), ARC (**G-H**) in the mouse brain from *Arl13b*$^{+/+}$ controls and *Arl13b*$^{A/A}$ mice. Scale bars 20µm and 5µm for insets indicated by white boxes. Hoechst-stained nuclei are blue.

Figure 2: Exclusion of ARL13B from cilia leads to obesity.

(A-B) Weekly male and female body weights from 3 to 10 weeks of age: *Arl13b*$^{+/+}$ (males n=14; females n=13), *Arl13b*$^{+/A}$ (males n=22; females n=22), *Arl13*$^{+/hnn}$ (males n=10; females n=9), *Arl13b*$^{A/A}$ (males n=24; females n=26), and *Arl13b*$^{A/hnn}$ (males n=15; females n=17). Data are presented as means ± SD. *P* values were determined by repeated measures ANOVA with Tukey's multiple comparisons test. **P* ≤ 0.01. (**C** and **H**) Lean mass and (**D** and **I**) fat mass of male and female control (*Arl13b*$^{+/A}$) and *Arl13b*$^{A/A}$. (**E** and **J**) Serum leptin levels. (**F** and **K**) Food intake. **(G** and **L**) Energy expenditure. Data are presented as means ± SD. N numbers indicated on graphs. Lean mass, fat mass, serum leptin, and food intake were analyzed using the Mann-Whitney U test. Energy Expenditure was analyzed by CalR ANCOVA, with body weight included as a covariate. ***P* < 0.01; ****P* < 0.001; ns, not significant with *P* > 0.05.

Figure 3: Insulin resistance and impaired glucose metabolism in *Arl13b*$^{A/A}$ mice

(**A-B**) Serum insulin levels in nonfasted 10-week-old male and female mice. Data points represent individual mice. Data are presented as means ± SD. Serum levels were analyzed using the Mann-Whitney U test. **P* ≤ 0.05; ***P* ≤ 0.01. (**C**-**D**) Glucose tolerance test in males and females. Blood glucose was measured at indicated times after i.p. glucose injection. (**E**-**F**) Insulin tolerance test of males and females. Blood glucose was measured at indicated times after i.p. insulin injection. The control group comprised pooled data from *Arl13b*$^{+/+}$, *Arl13b*$^{+/A}$, and

Arl13b$^{+/hnn}$ mice, and they did not differ in body weight. Data are presented as means ± SD. N numbers indicated on graphs. *P* values were determined by repeated measures ANOVA with Sidak's multiple comparisons test. *$P \leq 0.05$; **$P \leq 0.01$, ***$P \leq 0.001$; ****$P \leq 0.0001$; ns, not significant with $P > 0.05$.

Figure 4: ARL13B's GEF activity for ARL3 is not required for energy homeostasis.

(**A**-**B**) Body weights of adult male and female controls (*Arl13b*$^{+/+}$) and mutants (*Arl13b*$^{R79Q/R79Q}$). Data are presented as means ± SD. N numbers indicated on graphs. ns, not significant with Mann Whitney U test indicating $P > 0.05$.

Figure 5: Rescuing ciliary expression of ARL13B in adult mice prevents the metabolic phenotype of *Arl13b*$^{A/A}$ mice.

(**A**) Schematic of the *Arl13b-Fucci2a* conditional allele with tamoxifen Cre induction timeline. (**B-C**) Immunofluorescence of ADCY3 (red) and cerulean (cyan). (**B**) without Cre recombination. (**C**) with Cre-recombination. (**D-E**) Longitudinal body weight data of control, Arl*13b*$^{A/A}$, and Rescue (*Arl13b*$^{A/A}$*;AF2a; CAGG-CreER*^{T2}). Data are presented as means ± SD. N numbers indicated on graphs. *P* values were determined by repeated measures ANOVA with Tukey's multiple comparisons test. *$P \leq 0.01$. (**F-G**) Glucose tolerance test in males and females. Blood glucose was measured at indicated times after i.p. glucose injection. (**H-I**) Insulin tolerance test in males and females. Blood glucose was measured at indicated times after i.p. insulin injection. N numbers indicated on graphs. Data are presented as means ± SD. *P* values were determined by repeated measures ANOVA with Tukey's multiple comparisons test. *$P \leq 0.05$; **$P \leq 0.01$; ***$P \leq 0.001$; ns, not significant with $P > 0.05$.

578

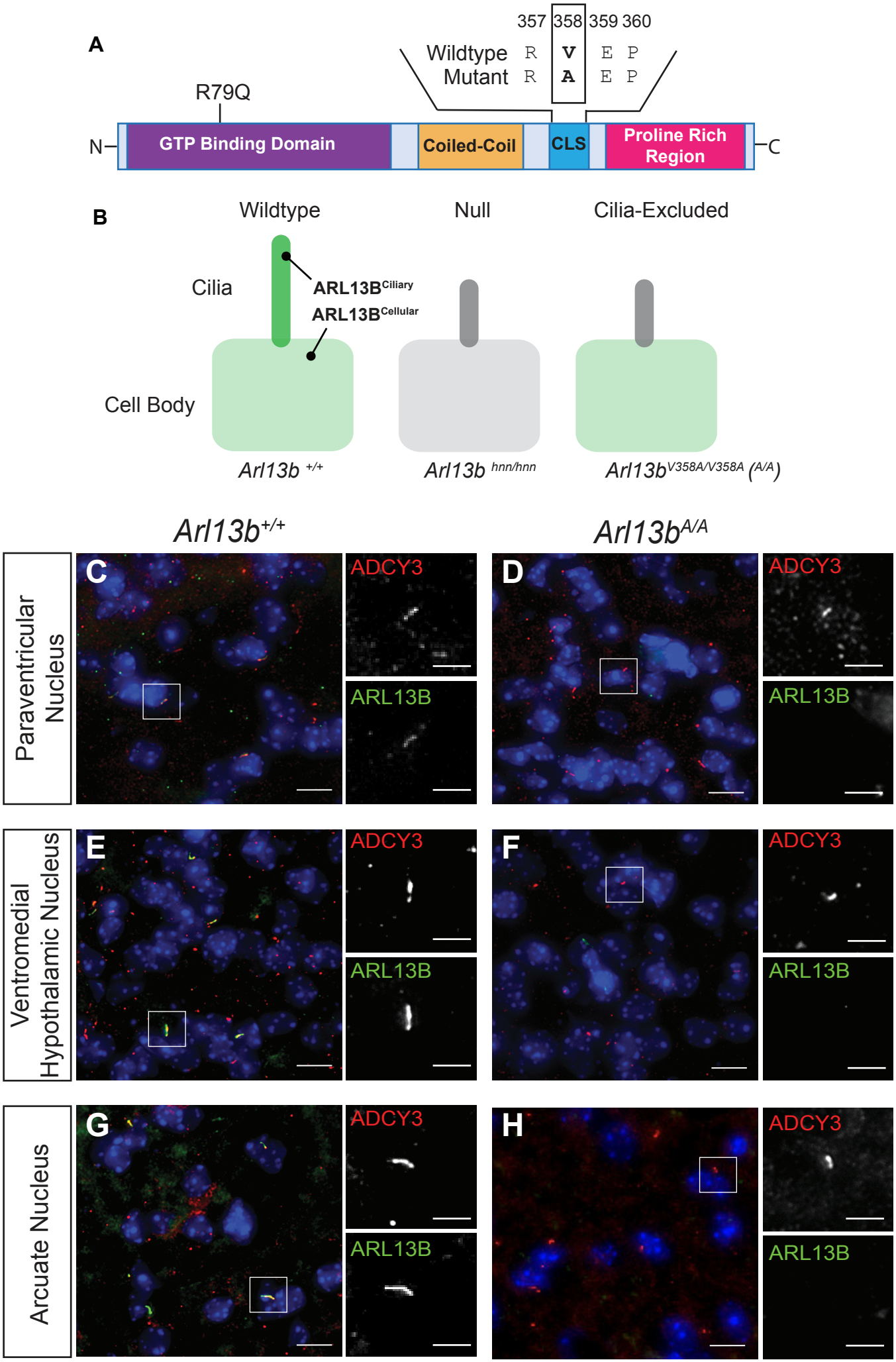
A
357 358 359 360
Wildtype R V E P
Mutant R A E P
R79Q
N
GTP Binding Domain
Coiled-Coil
CLS
Proline Rich Region
C
B
Wildtype
Null
Cilia-Excluded
Cilia
ARL13B Ciliary
ARL13B Cellular
Cell Body
Arl13b +/+
Arl13b hnn/hnn
Arl13b V358A/V358A (A/A)
Arl13b+/+
Arl13bA/A
Paraventricular Nucleus
Ventromedial Hypothalamic Nucleus
Arcuate Nucleus
C
D
E
F
G
H
ADCY3
ARL13B

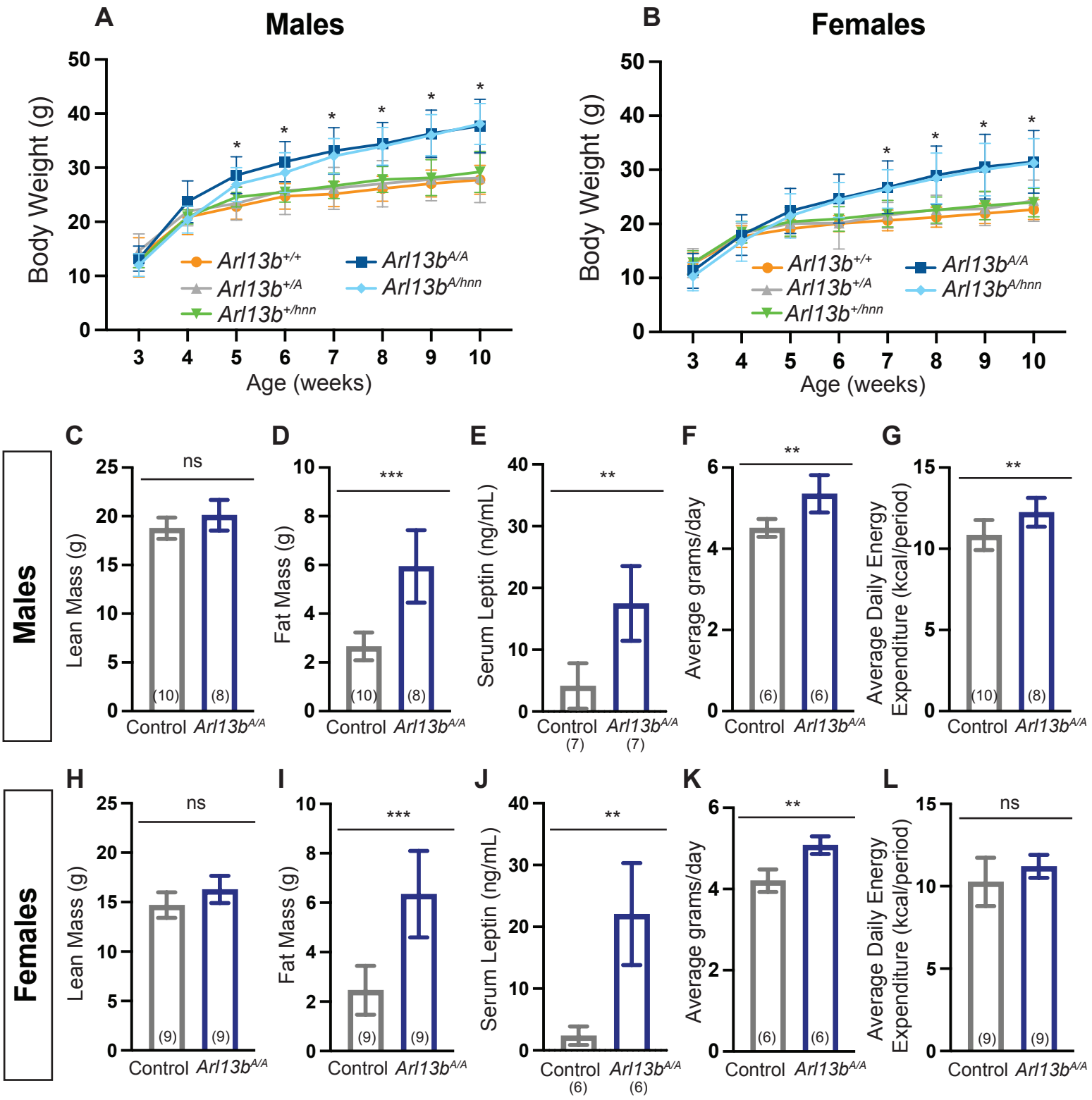
A
Males
Body Weight (g)
Age (weeks)
Arl13b+/+
Arl13b+/A
Arl13b+/hnn
Arl13bA/A
Arl13bA/hnn
B
Females
Body Weight (g)
Age (weeks)
Males
C
Lean Mass (g)
ns
(10)
(8)
Control
Arl13bA/A
D
Fat Mass (g)
***
(10)
(8)
E
Serum Leptin (ng/mL)
**
(7)
(7)
F
Average grams/day
**
(6)
(6)
G
Average Daily Energy Expenditure (kcal/period)
**
(10)
(8)
Females
H
Lean Mass (g)
ns
(9)
(9)
I
Fat Mass (g)
***
(9)
(9)
J
Serum Leptin (ng/mL)
**
(6)
(6)
K
Average grams/day
**
(6)
(6)
L
Average Daily Energy Expenditure (kcal/period)
ns
(9)
(9)

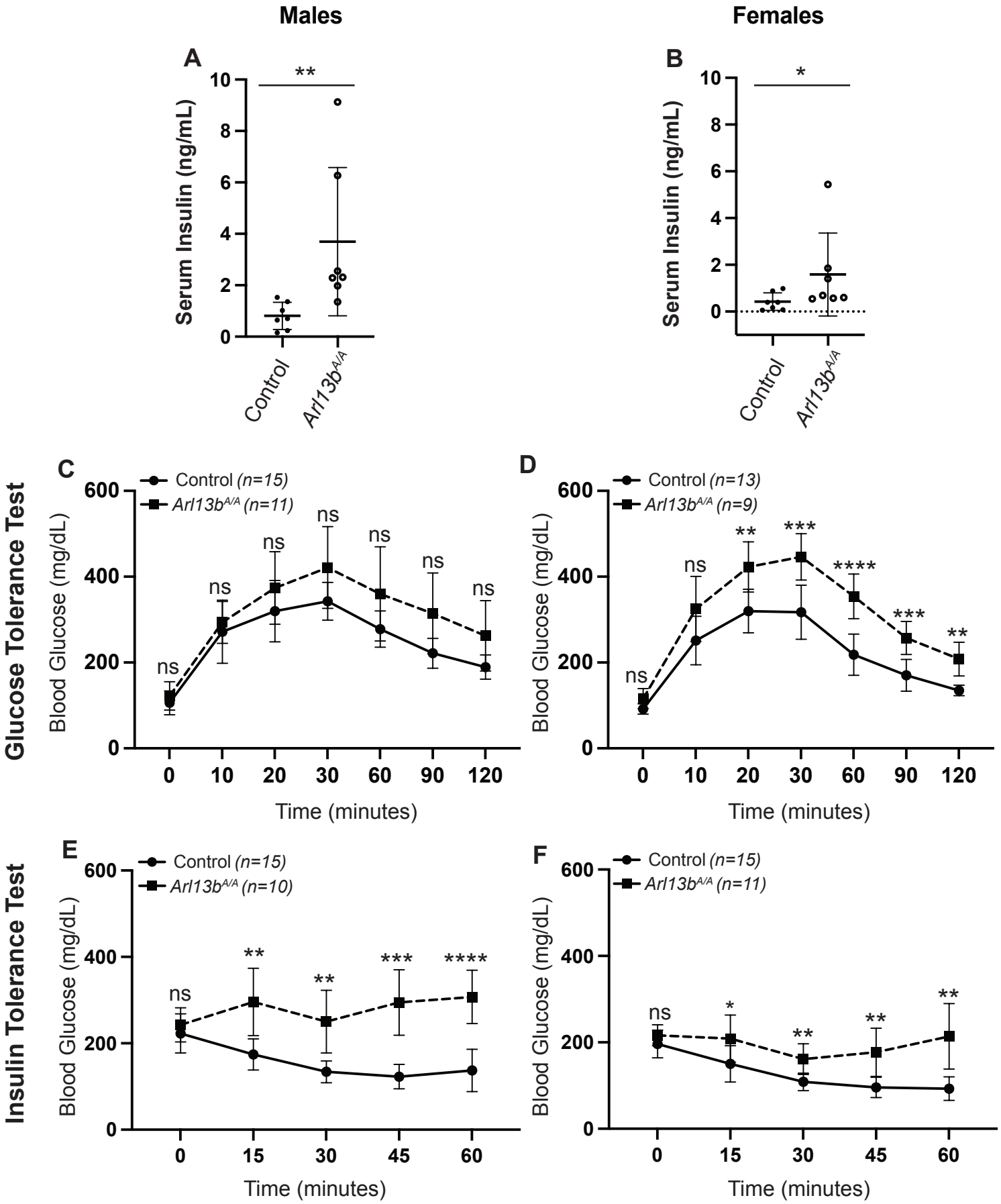
Males
Females
A
B
Serum Insulin (ng/mL)
Control
Arl13b A/A
C
D
Glucose Tolerance Test
Control (n=15)
Arl13b A/A (n=11)
Control (n=13)
Arl13b A/A (n=9)
Blood Glucose (mg/dL)
Time (minutes)
E
F
Insulin Tolerance Test
Control (n=15)
Arl13b A/A (n=10)
Control (n=15)
Arl13b A/A (n=11)

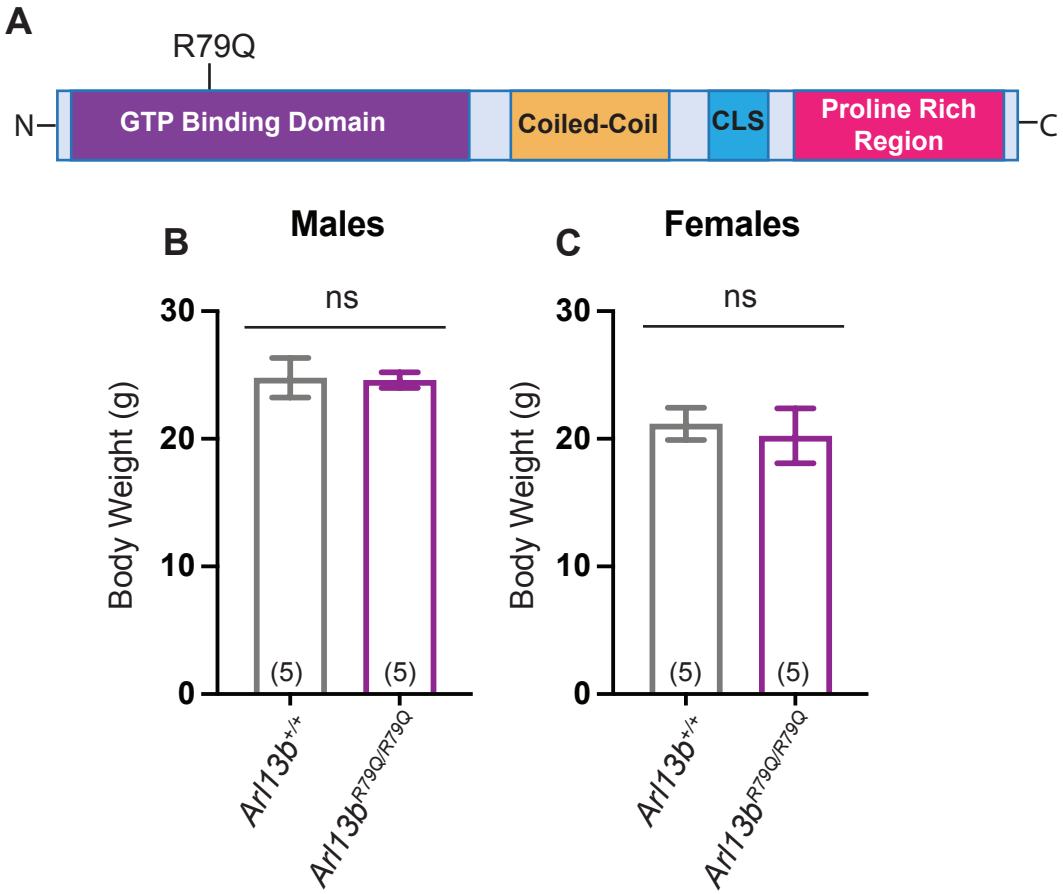
A
R79Q
N
GTP Binding Domain
Coiled-Coil
CLS
Proline Rich Region
C
B
Males
ns
Body Weight (g)
30
20
10
0
(5)
(5)
Arl13b+/+
Arl13bR79Q/R79Q
C
Females
ns
Body Weight (g)
30
20
10
0
(5)
(5)
Arl13b+/+
Arl13bR79Q/R79Q

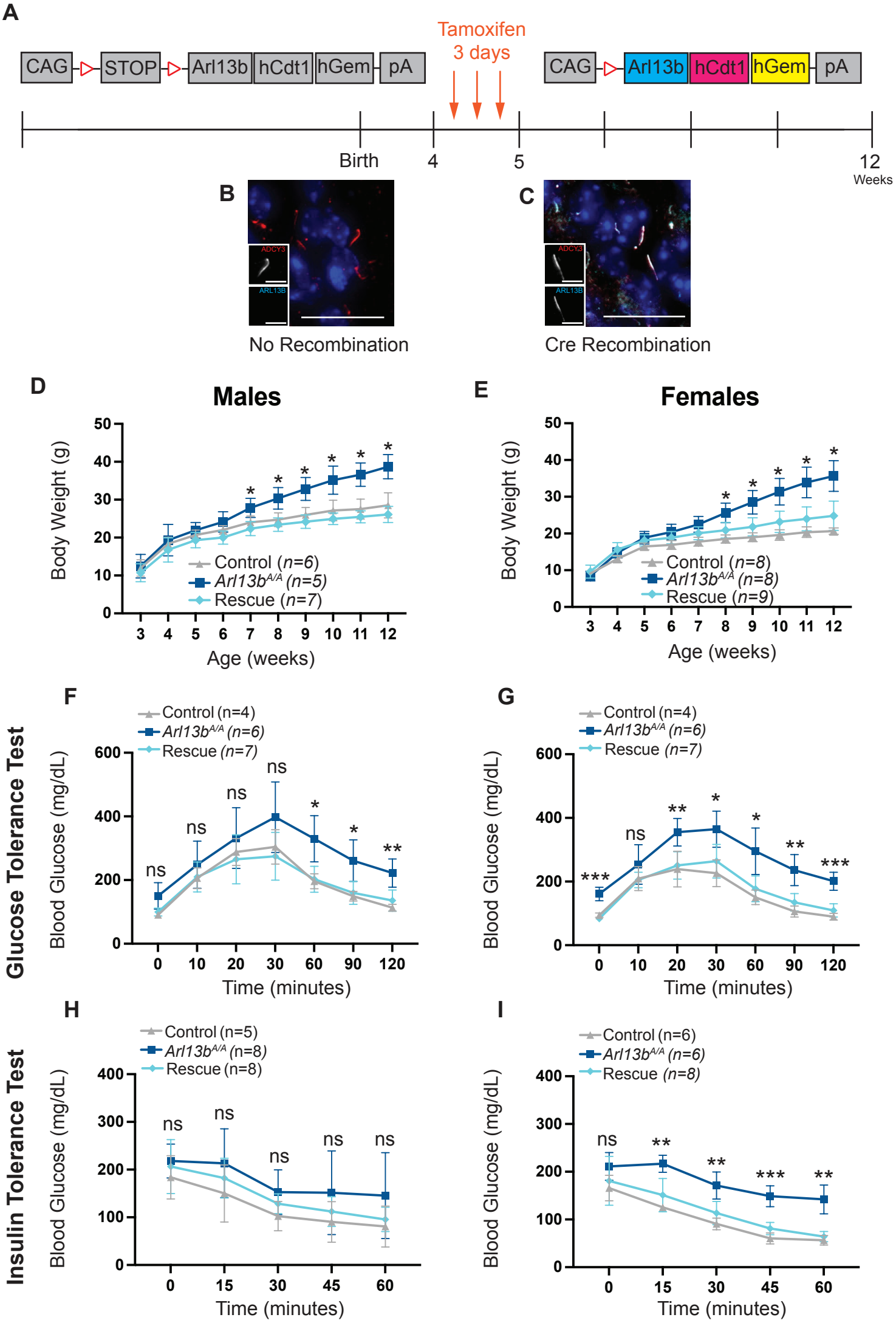
A
CAG
STOP
Arl13b
hCdt1
hGem
pA
Tamoxifen
3 days
CAG
Arl13b
hCdt1
hGem
pA
Birth
4
5
12
Weeks
B
ADCY3
ARL13B
No Recombination
C
ADCY3
ARL13B
Cre Recombination
D
Males
Body Weight (g)
Control (n=6)
Arl13b^A/A (n=5)
Rescue (n=7)
Age (weeks)
E
Females
Body Weight (g)
Control (n=8)
Arl13b^A/A (n=8)
Rescue (n=9)
Age (weeks)
Glucose Tolerance Test
F
Control (n=4)
Arl13b^A/A (n=6)
Rescue (n=7)
Blood Glucose (mg/dL)
Time (minutes)
G
Control (n=4)
Arl13b^A/A (n=6)
Rescue (n=7)
Blood Glucose (mg/dL)
Time (minutes)
Insulin Tolerance Test
H
Control (n=5)
Arl13b^A/A (n=8)
Rescue (n=8)
Blood Glucose (mg/dL)
Time (minutes)
I
Control (n=6)
Arl13b^A/A (n=6)
Rescue (n=8)
Blood Glucose (mg/dL)
Time (minutes)